PHYSICAL REVIEW B VOLUME 45, NUMBER 1 1 JANUARY 1992-I

Pressure-induced phase transformations in alkali-metal hydrides calculated using an improved linear-muffin-tin-orbital–atomic-sphere-approximation energy scheme

C. O. Rodriguez* and M. Methfessel†

Max-Planck Institut für Festkörperforschung, Heisenbergstrasse 1, D-7000 Stuttgart 80, Germany

(Received 27 September 1990; revised manuscript received 27 June 1991)

A scheme for the calculation of total energies from first principles is described which is intermediate between the popular linear muffin-tin-orbital method in the atomic-sphere approximation (LMTO-ASA) and an exact full-potential treatment. The local-density total energy is evaluated accurately for the output charge density from the ASA potential. This method is applied to the study of static structural properties and the pressure-induced phase transformation from $B1$ (NaCl-structure) to $B2$ (CsCl-structure) phases for the partially ionic alkaki-metal hydrides NaH and KH and the alkali halide NaCl. Good agreement with experimental transition pressures and volumes is obtained. The series NaH, KH, and NaCl shows the observed strong cation and weak anion dependence. Charge densities and band structures are given at zero and high pressure. Calculated energy-volume curves for LiH show no transition up to 1 Mbar, in agreement with experimental data.

I. INTRODUCTION

With the exception of LiH, the series of partially ionic alkali-metal hydrides transforms from the $B1$ to the $B2$ structure at transition pressures P_t ranging from 4 to 300 kbar.[1] Recent high-pressure studies with the diamond anvil cell for NaH (Ref. 2) have completed the data for the series and have enabled a systematic comparison of transition pressures as well as equations of state, bulk moduli, and effective charges with those of alkali-metal halides. These results show that there is a strong cation and weak anion dependence of the observed P_t for the $B1$-to-$B2$ transition. LiH will transform at a pressure above current capability, if at all.[3,4]

From the theoretical side a number of different approaches exist. On the one hand, hard-sphere ion models,[5,6] in which a complete charge transfer between the ions is assumed, predict specific volumes for the $B1$ and $B2$ phases[5] and bulk moduli.[6] Since much of the experimental evidence points to the fact that the effective charge on each ion is less than $\pm 1e$, the work of Anderson and Nafe[7] and Jarayaman, Batlogg, and Maines[8] uses an ionic model that incorporates effective ion charges. They explain the behavior of the bulk modulus for the different compounds in the $B1$ phase as a function of the equilibrium unit-cell volume by postulating an effective charge $Z_{\text{eff}}=(B/B_A)^{1/2}$, where B/B_A is the bulk modulus ratio of the alkali-metal hydrides and alkali-metal halides. For the latter a complete charge transfer is assumed. The idea of an incomplete transfer for the hydrides is consistent with the fact that there is a smaller electronegativity difference for these. Calder *et al.*[9] have used data from x-ray measurements to deduce LiH to be 80–100 % ionic, and neutron-diffraction experiments indicate approximately 90% ionic bonding in LiH.[10]

For the special case of LiH, a number of theoretical studies have been made concerning the electronic structure and equation of state and related properties.[11–17] In particular, effects of pressure and the possibility of an insulating-metallic transition have been addressed by a number of groups.[15,18]

Within a tight-binding theory and without assumptions concerning ionicity, Majeswski and Vogl[19] have given a qualitative explanation of why the transition pressure $P_t=\Delta E/\Delta E$ is highly dependent on the cation and nearly independent of the anion for the case of sp-bonded compounds.

Motivated by recent results on NaH, already mentioned,[2] which completed previous studies on the series by Hochheimer *et al.*,[1] we address in this paper, in more detail (a preliminary study has already been reported[16]), the question of determining transition pressures and structurally related properties of NaH and KH by using a recently developed atomic-sphere-approximation plus total energy E evaluation (ASA+E) scheme within the linear-muffin-tin-orbital (LMTO) formalism. First-principles calculations are done in the framework of the local-density approximation (LDA) to evaluate the total energy of the crystal for the $B1$ and $B2$ structures at different volumes. In addition to NaH, KH, and LiH, we have also studied NaCl to see if the strong cation and weak anion dependence of the transition pressure can be reproduced. All calculated structural properties and transition pressures are in good agreement with experiment. A detailed study of charge densities and band structures as a function of pressure is made. A qualitative discussion of charge transfer is given. Similar studies for NaCl and KCl (Ref. 20) and the hydrides series,[17] using *ab initio* pseudopotentials, have also been reported. Reference 20 also addresses the important issue of zero-point motion effects.

The idea of the ASA+E scheme is to use the standard LMTO-ASA method to first generate a reasonably accurate potential, which correctly describes overall effects such as charge transfer between atoms. In the second step, a modified LMTO method is used to calculate the LDA total energy for the charge density obtained by solving the Schrödinger equation in this potential. All the approximations of the ASA, such as the spheridization of the output density, are avoided in the second step. Because of the variational principle, we expect to obtain accurate total energies in this way. Our denotation "ASA+E" reflects this philosophy of appending an accurate total-energy determination to a standard LMTO-ASA calculation.

The paper is organized as follows. Details of the calculation are given in Sec. II. In Sec. III results are given, including energy bands, charge densities, and predicted transition pressures for NaH, KH, and NaCl in both the *B*1 and *B*2 structures. Results for LiH will also be addressed. The conclusions of this work are summarized in Sec. IV.

II. CALCULATION METHOD

The ground-state properties and transition pressures are obtained by calculating the total energy of the system within the LDA approximation to the density-functional formalism and using the Kohn-Sham self-consistent-field procedure.[21] We expand the one-electron orbitals in LMTO's.

The LMTO method belongs to the class of linear band-structure methods and uses a muffin-tin (MT) potential to define a small, dedicated basis set for solving the Schrödinger equation for the solid. The LMTO orbitals are eigenfunctions of ∇^2, that is, Hankel functions of kinetic energy κ^2 times a spherical harmonic, in the interstitial region. These multipole-field-envelope functions are augmented continuously and differentiably within MT spheres by means of the solution of the radial Schrödinger equation at a fixed energy and its first energy derivative.

For crystals the standard LMTO method uses a single-κ basis (in particular $\kappa^2=0$). In the ASA the MT spheres are chosen as space-filling Wigner-Seitz (WS), slightly overlapping spheres. If the structure is not close packed, empty spheres and associated LMTO-basis functions can be centered at interstitial sites, in addition to those centered at the atoms. The Coulomb and exchange-correlation energies are calculated after the charge density has been spherically averaged inside the WS spheres. If the amount of overlapp is smaller than 15–20 %, this method has proven to yield accurate results for electronic properties and leads to highly efficient computer programs. But because of the approximations to the potential and charge density, in the ASA the calculation of energy differences caused by symmetry-lowering displacements of atoms is not possible and only in some special cases can the method be used for the study of stability curves between different phases.

Within the LMTO framework it is now possible to obtain the total energy of the system when both the potential and charge density are permitted to have a completely general form. These implementations are referred to as a full-potential (FP) LMTO and have been applied successfully to a number of different systems.[22] Of course, additional complexity and computing effort is required by this kind of approach. On the other hand, the output charge density for an ASA potential is known to be highly accurate, and treating the potential in a completely general form may not be necessary for some applications.

In a typical calculation for pressure phase transitions using the LMTO-ASA approach, the energy-volume curve for each separate phase will have the correct shape (giving the correct equilibrium volume and bulk modulus), but the curves are shifted in energy relative to each other. On the other hand, the true crystal potential is very similar to the potential V_{ASA} from a self-consistent ASA calculation if the latter is interpreted in the following way:[23] Inside sphere ν, V_{ASA} is equal to the spherical potential V_ν; in the interstitial region, V_{ASA} is the muffin-tin zero V_{MTZ}; in the overlap of spheres ν and μ, V_{ASA} is equal to $V_\nu+V_\mu-V_{\mathrm{MTZ}}$. The question arises whether a careful evaluation of all energy terms for this potential can yield total energies in good agreement with those of a full-potential calculation. This hope is based on the variational principle for the local-density total energy, which states that errors in the total energy are second order in the deviation of the input potential from the true self-consistent potential. Two types of error are present when a straightforward ASA is used: (1) errors in the overlap and kinetic-energy errors because of double augmentation in the overlap regions and (2) errors caused by the spherical approximation to the charge density when the Coulomb and exchange-correlation energies are calculated. In order to get a clear answer about the effect of these errors, the ASA+E scheme was designed to eliminate both types. All remaining differences to the full-potential results must then be caused by the deviation of V_{ASA} from the true self-consistent potential.

The ASA+E scheme starts from a self-consistent ASA calculation. In a final added iteration, nonoverlapping muffin-tin spheres are introduced in addition to the space-filling ASA spheres. As in the FP-LMTO method, a basis set is constructed by augmenting the envelope functions inside the muffin-tin spheres. To get a more complete basis in the (now nonvanishing) interstitial region, a double- or triple-κ set is used. A point worth emphasizing is that the matrix elements can be calculated using the standard and efficient LMTO-ASA techniques for the potential V_{ASA} defined above. This is done by means of a special augmentation procedure which we have developed. It is closely related to the standard approach, which is to substitute for an envelope function inside the ASA sphere a linear combination of ϕ and $\bar{\phi}$, which matches smoothly at the sphere boundary. Hereby, ϕ and $\bar{\phi}$ are the solutions of the Schrödinger equation for the spherical ASA potential and their energy derivatives, respectively. In our case we want to treat the space between the muffin-tin and ASA radii in such a way that multiple overlaps no longer cause any error. Therefore, we define the augmentation of a function (Hankel or Bessel) to be simply equal to that same function between R_{MT} and R_{ASA} and to be a linear combination of ϕ and $\bar{\phi}$ inside R_{MT}. The coefficients are now chosen to get smooth matching at R_{MT}. Hamiltonian and overlap integrals over the ASA spheres are calculated for these functions, which then are combined with structure constants as in the normal ASA procedure with the combined-correction terms included. The muffin-tin radius is only needed to calculate modified potential parameters (here expressed as integrals over the augmentation functions); the rest of the procedure operates with overlapping ASA spheres as usual. Between R_{MT} and R_{ASA}, the modified augmentation scheme replaces the envelope function by itself, so that multiple augmentation in the overlap regions does not lead to ambiguities. Our procedure has the following property: It calculates exactly the Hamiltonian (and overlap) matrix elements for the potential made by overlapping spherical potentials, for a basis of LMTO's defined with respect to nonoverlapping muffin-tin spheres. The effort is the same as that of a standard ASA calculation: In either case the matrix elements are made by combining integrals over the spheres with the structure constants. The essence of the procedure is that the augmentation from within one sphere adds the contribution from the potential inside that sphere, so that the final result corresponds to the overlapped sum of all the potentials. Our scheme makes it possible to treat efficiently and accurately a special type of potential, namely, overlapped (and, with slight modifications, nonspherical) potentials defined within ASA spheres.

The second ingredient of the ASA+E procedure is to evaluate properly and without spheridization the electrostatic and exchange-correlation total-energy terms. For this we use the techniques developed for the full-potential LMTO method of Ref. 24. The charge density (including the nonspherical part) is accumulated inside the muffin-tin spheres. The interstitial density is taken as a linear combination of Hankel functions which matches the sphere density smoothly. The exchange-correlation energy density is treated in a similar way. The Hankel-function representation makes it easy to solve the Poisson equation and to calculate the total-energy contributions from the interstitial. For geometries with a small interstitial region, this method permits a fast and accurate evaluation of the total energy.

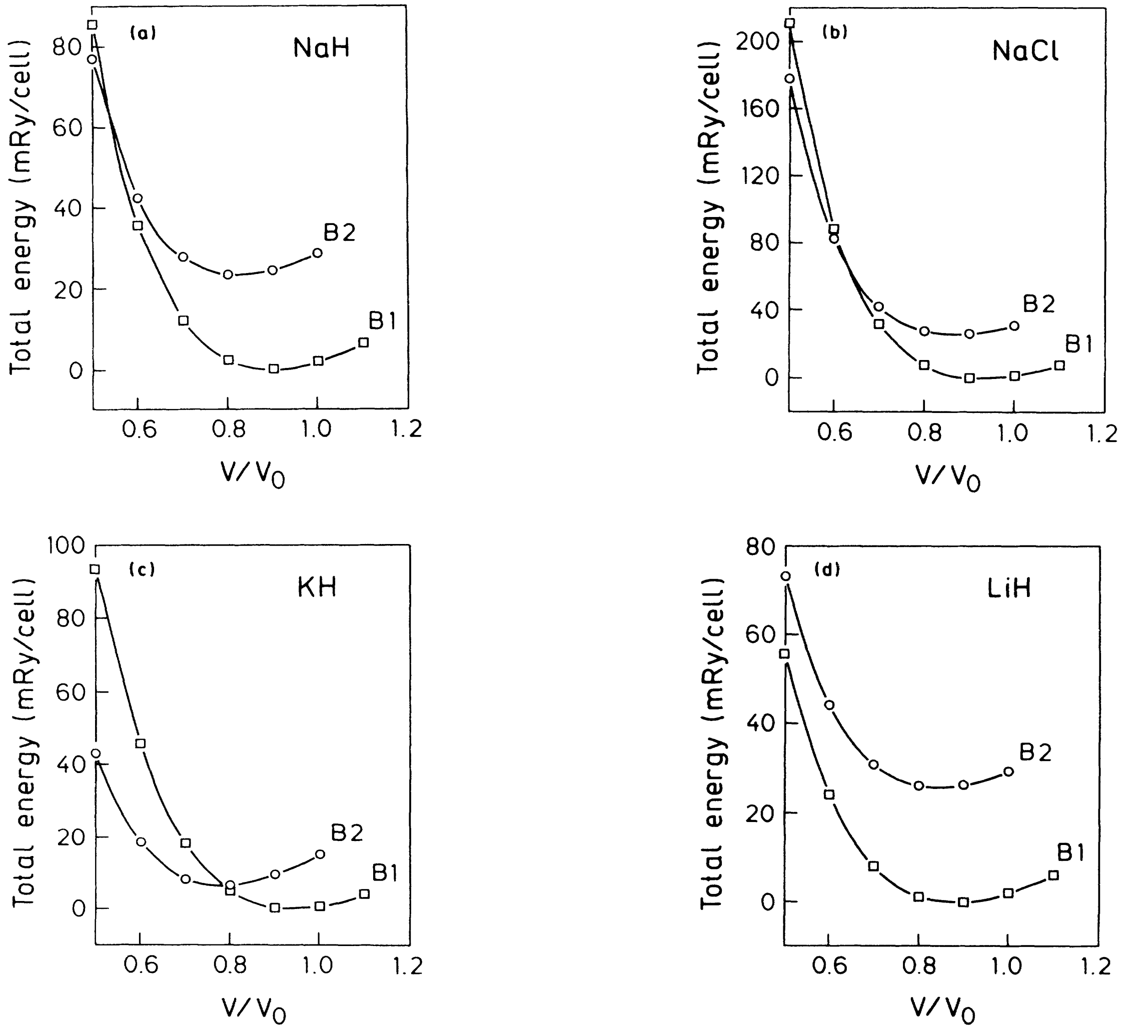

FIG. 1. Calculated total energies per unit cell for $B1$ and $B2$ structures as a function of volume. (a) NaH, (b) NaCl, (c) KH, and (d) LiH. Solid lines are a guide to the eye through the calculated points. V_0 is taken as the experimental cell volume for the $B1$ structure at $T=0$ and atmospheric pressure.

TABLE I. Static properties of LiH, NaH, KH, and NaCl.

	Expt.	Present calc.	Other calc. *A*	Other calc. *B*
LiH				
Lattice constant (Å)	4.06[a]	3.94	3.93[b]	
			3.34[c]	3.60[c]
			3.89[d]	4.03[d]
Bulk modulus (Mbar)	0.32[e]	0.40	0.43[b]	
			0.66[c]	0.53[c]
			0.40[d]	0.31[d]
NaH				
Lattice constant (Å)	4.88[f]	4.71	4.77[d]	4.92[d]
Bulk modulus (Mbar) *B*1	0.19[f]	0.28	0.27[d]	0.20[d]
Bulk modulus (Mbar) *B*2	0.28[f]	0.28		
KH				
Lattice constant (Å)	5.71[g]	5.61	5.83[d]	5.99[d]
Bulk modulus (Mbar)	0.16[g]	0.19	0.15[d]	0.12[d]
NaCl				
Lattice constant (Å)	5.60[h]	5.49	5.52[i]	
Bulk modulus (Mbar) *B*1	0.27[j]	0.33	0.31[i]	

[a] Reference 26.
[b] Reference 13.
[c] Reference 11.
[d] Reference 17.
[e] Reference 27.
[f] Reference 2.
[g] Reference 1.
[h] Reference 28.
[i] Reference 20.
[j] Reference 29.

Overall, the efficiency of the scheme is intermediate between that of a standard ASA and a full-potential LMTO calculation. The added step for evaluating the total energy requires an effort which is about equal to that of one iteration using the full-potential method. Therefore, the deciding factor is the number of iterations which are needed to attain self-consistency. For large and complex systems, this number is quite large, so that the ASA+E scheme is then about as efficient as the standard approach.

All the calculations presented here were done with a double-κ $(2xs,2xp,2xd)$ basis set in the final iteration. The muffin-tin spheres were slightly smaller than touching, and no empty spheres were needed. The Brillouin-zone integration used ten special $\bar{k}$-points in the irreducible segment of the Brillouin zone. The Hedin-Lundqvist parametrization was used for exchange and correlation. For the case of KH in the $B2$ structure, a two-panel calculation was needed since the large size of the potassium ion leads to second-neighbor core-core overlap. This will be discussed further later. The final total energy was converged to 1 mRy/cell with respect to increase of the basis for both phases. In the ASA part, the calculations were iterated to self-consistency until energies were stable to 10^{-4} Ry/cell.

III. RESULTS AND DISCUSSION

In Fig. 1 the calculated total energies E_{tot} for NaH, KH, NaCl, and LiH are shown for the two phases studied: $B1$ (NaCl-structure) and $B2$ (CsCl-structure) phases. The energies are expressed as a function of the volume normalized to the experimental volume V_0 of the $B1$ phase. NaCl was also studied since part of our interest was in the possibility of predicting the strong cation and weak anion dependence of the $B1$-to-$B2$ transition pressures.

The equilibrium structural properties are obtained by fitting to Birch's[25] equation of state and are listed in Table I compared to experimental values and those of pseudopotential calculations. The results agree well with experimental values. As shown by Martins (column B in Table I, from Ref. 17), these could be further improved by correcting for zero-point motion effects; as pointed out in Refs. 12 and 20, the lattice constant will increase, while the bulk modulus will decrease. In the case of LiH, the results of Ref. 11 are obtained using norm-conserving pseudopotentials with the 1*s* electrons of Li treated as core electrons, thus not including the nonlinear exchange and correlation interaction between the core and valence densities.[30] In the pseudopotential calculation of Ref. 13, all electrons were included in the context of exchange and correlation, and these results show good agreement with our present calculation. We mention that the computational effort in the present scheme is much smaller than when pseudopotentials and plane-wave expansions are used, because of the problems associated with the hydrogen potential.

As pressure is increased (in our calculation hydrostatic compression applied), most alkali-metal hydrides undergo a phase transformation from the $B1$ to the $B2$ phase. From the common tangent of the two calculated energy-volume curves, the transition pressure is deduced. The values of P_t and transition volumes v_{B1} and v_{B2} are listed in Table II. In the case of LiH, no attempt was made to calculate P_t since the transition will occur (if it does) at

TABLE II. Transition pressures and transition volumes for the $B1$-$B2$ transformation in NH, NaCl, and KH. The volumes are given as fractions of the room-temperature zero-pressure volume. ΔV is the volume change at the transition pressure.

	NaCl		NaH		KH	
	calc.	expt.[a]	calc.	expt.[b]	calc.	expt.[c]
P_t (kbar)	265	290	307	293	20	40
V_{B1}	0.65	0.64 0.65 0.63–0.70	0.57	0.61	0.85	0.82
V_{B2}	0.61	0.61 0.62 0.60–0.64	0.52	0.55	0.71	0.71
$\Delta V/V_{B1}$ (%)	−6.6	−5.8 −5.0 −1.3	−8.8	−10.0	−16.4	−13.4

[a] Reference 20 and references cited therein.

[b] Reference 2.

[c] Reference 1.

volumes of the order of $0.4V_0$ (i.e., outside the volume range considered here), with pressures of the order of 1 Mbar. As can be seen from Table II, the agreement to the measured transition data is good and the experimental fact of a strong cation dependence on P_t (i.e., in the case of NaH, and the P_t of KH goes from $\cong 300$ to $\cong 20$ kbar) and weak anion dependence (i.e., for both NaH and NaCl, $P_t \cong 300$ kbar) is well reproduced. In the case of KH, the error in P_t is of the order of 20 kbar, since a change of the $B2$ curve of 1 mRy (which is the error for our calculated E_{tot}) changes P_t by this amount.

The calculated band structures for NaH (in the $B1$ structure) and KH (in the $B2$ structure) are given in Figs. 2 and 3 at the volumes $V=1.0V_0$ and $0.6V_0$. In these figures the Na $2p$ and K$3p$ semicore states are included. At a given volume the second-nearest-neighbor distance (i.e., Na-Na, K-K) is smaller in the $B2$ than in the $B1$ structure. Consequently, the semicore dispersion is larger in the $B2$ than in the $B1$ structure. This effect becomes more drastic as pressure is applied. For example, in the case of NaH at volume $V=V_0$, these bands are dispersionless for the $B1$ phase, but exhibit a small dispersion for the $B2$ structure. When the volume is reduced to $V=0.6V_0$, the broadening increases, this effect being larger for the $B2$ phase. In the case of KH (Fig. 3), the dispersion becomes so large that the $3p$ state must be treated with the same methods as the valence states (i.e., by a two-panel calculation, as mentioned earlier). The dispersion for $V=V_0$ in both structures is already noticeable ($\cong 20$ mRy in the $B2$ structure). The dispersion goes up to $\cong 200$ mRy for the $B2$ case in the pressure range we have considered.

The effect of broadening of the semicore bands with pressure is also evident when a study of the charge distribution is done. Figure 4 shows contour plots for the valence and total charge densities of NaH at volumes $V=V_0$ and $V=0.6V_0$. As can be seen, H has become negatively charged, whereas Na has lost a part of its valence electron. To quantify this is very difficult since a measure of ionicity or charge transfer is somewhat arbitrary (unless the system is totally ionic, which is not the case here). In any case we can divide space by means of equal-sized muffin-tin spheres around the atoms and study the flow of charge from one sphere to the other and to the interstitial as pressure is applied. In the case of NaH, pressure leads to redistribution of charge for both phases, but the flow of charge between Na and H is small.

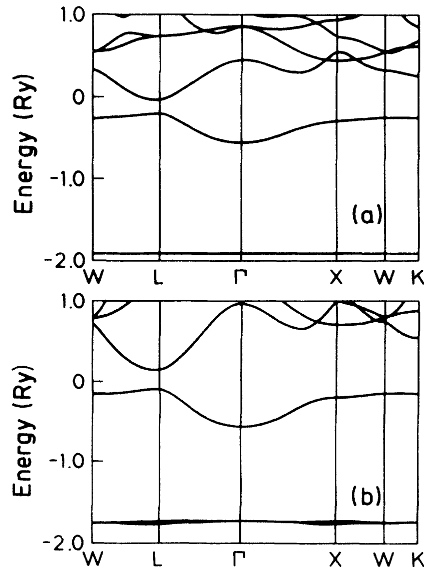

FIG. 2. Band structure for NaH in the $B1$ structure for volumes (a) $V=V_0$ and (b) $V=0.6V_0$.

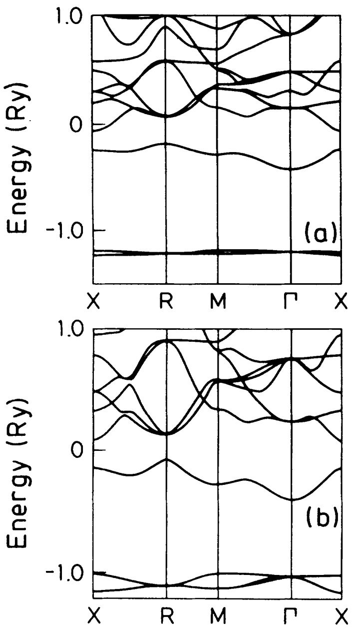

FIG. 3. Band structure for KaH in the $B2$ structure for volumes (a) $V=V_0$ and (b) $V=0.6V_0$.

On the other hand, in the case of KH, charge spills out of the MT spheres with increasing pressure and is transferred from K to H. The spillout is a consequence of the large $3p$-$3p$ overlap, which was evident in the broad semicore band. We mention that the problem of the K-K semicore overlap was already pointed out in the pseudopotential calculation of Ref. 20 for alkali halides, although the effect was smaller since the lattice constants of the halides are larger than those of the hydrides.

IV. CONCLUSION

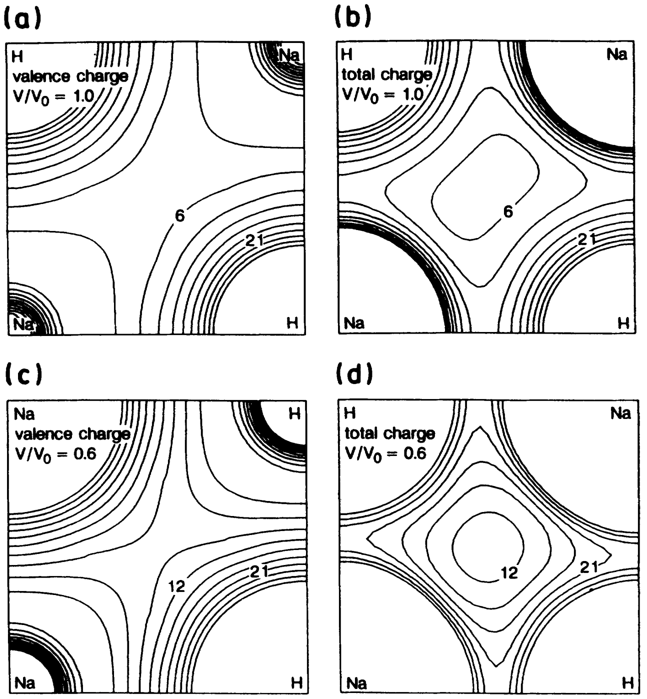

FIG. 4. Charge-density distribution for NaH in the 100 plane. Panels (a) and (c) correspond to valence charge at $V=V_0$ and $V=0.6V_0$, respectively; (b) and (d) correspond to the total charge at the same volumes. Units are milielectrons/a.u.^{3} in steps of 3.

A LMTO scheme which is intermediate between between the standard LMTO-ASA and an exact full-potential treatments was used for the calculation of LDA total energies in the alkali-hydrides series. For a self-consistent ASA potential, a multiple-κ LMTO basis with augmentation inside nonoverlapping muffin-tin spheres was used in a final total-energy iteration. Hereby, the total energy was evaluated for the ASA potential, but without the errors associated with multiple augmentation in the overlap regions and the spheridization of the charge density in the electrostatic and exchange-correlation energy terms. The application to energy-volume curves of LiH, NaH, KH, and NaCl in the $B1$ and $B2$ structures showed that for these symmetric structures the scheme gives results as accurate as full-blown full-potential methods. We conclude that the difference between the ASA and true self-consistent potentials is small enough for the variational principle to reduce the total-energy error to negligible size. Calculated ground-state properties and transition pressures and volumes agree well with available experimental data. The observed cation or anion dependence of the transition pressure is reproduced. In our calculations a major difference between hydrides containing Na and K is that the overlap between K $3p$ semicore states from second-nearest neighbors is much greater than that between Na $2p$ states. Because of the different second-nearest-neighbor distance in the $B1$ and $B2$ structures, a semicore band of considerable width is found in the $B2$ but not in the $B1$ structure.

ACKNOWLEDGMENTS

This work has benefited from discussion with O. K. Andersen, K. Kunc, N. Christensen, P. Plöchl, and G. P. Das.

---

*Present address: Instituto de Física de Líquidos y Sistemas Biológicos (IFLYSIB), C.C. 565, La Plata (1900), Argentina.

†Present address: Fritz Haber Institüt, Faradayweg 4-6, D-1000 Berlin, FRG.

[1] H. D. Hochheimer, K. Strössner, W. Hönle, B. Baranowski, and F. Filipek, Z. Phys. Chem. **143**, 139 (1985).

[2] S. J. Duclos, Y. K. Vohra, and A. L. Ruoff, Phys. Rev. B **36**, 7664 (1987).

[3] D. R. Stephens and E. M. Lilley, J. Appl. Phys. **39**, 177 (1968).

[4] Y. Kondo and K. Asuami, J. Phys. Soc. Jpn. **57**, 367 (1988).

[5] I. O. Bashkin, T. N. Dymova, and E. G. Ponyatouskii, Phys. Status Solidi B **100**, 87 (1980).

[6] B. R. Gupta and V. Kumar, Czech J. Phys. B **33**, 1011 (1983).

[7] O. L. Anderson and J. E. Nafe, J. Geophys. Res. **70**, 3951 (1965).

[8] A. Jayaraman, B. Batlogg, and R. G. Maines, Phys. Rev. B **26**, 3347 (1982).

[9] R. S. Calder, W. Cochran, D. Griffiths, and R. D. Lowde, J. Phys. Chem. Solids **23**, 621 (1962).

[10] J. L. Verble, J. L. Warren, and J. L. Yarnell, Phys. Rev. **168**, 980 (1968).

[11] C. O. Rodriguez and K. Kunc, Solid State Commun. **64**, 19 (1987).

[12] C. O. Rodriguez and K. Kunc, J. Phys. Condens. Matter **1**, 1601 (1989).

[13] K. Kunc, J. Chem. Phys. **86**, 647 (1989).

[14] F. Perrot, Phys. Status Solidi B **77**, 517 (1976).

[15] J. Hama and N. Kawakami, Phys. Lett. A **126**, 348 (1988).

[16] C. O. Rodriguez, M. Methfessel, and O. K. Andersen, Bull. Am. Phys. Soc. **34**, 545 (1989).

[17] J. L. Martins, Phys. Rev. B **41**, 7883 (1990).

[18] N. I. Kulikov, Fiz. Tverd. Tela (Leningrad) **20**, 2027 (1978) [Sov. Phys. Solid State **20**, 1170 (1978)].

[19] J. A. Majewski and P. Vogl, Phys. Rev. Lett. **57**, 1366 (1986).

[20] S. Froyen and M. L. Cohen, J. Phys. C **19**, 2623 (1986).

[21] P. Hohenberg and W. Kohn, Phys. Rev. **136**, B864 (1964); W. Kohn and L. J. Sham, *ibid.* **140**, A1133 (1965); L. J. Sham and W. Kohn, Phys. Rev. B **145**, 561 (1966).

[22] M. Methfessel, C. O. Rodriguez, and O. K. Andersen, Phys. Rev. B **40**, 2009 (1989).

[23] O. K. Andersen, M. Methfessel, C. O. Rodriguez, P. Blöchl, and H. M. Polatoglou, in *Atomistic Simulation of Materials,* edited by D. J. Srolovitz and V. Vitek (Plenum, New York, 1989), p. 1.

[24] M. Methfessel, Phys. Rev. B **38**, 1537 (1988).

[25] F. B. Birch, J. Geophys. Res. **83**, 1257 (1978).

[26] J. P. Vidal and G. Vidal-Valat, Acta Crystallogr. B **42**, 131 (1986).

[27] D. Gerlich and C. S. Smith, J. Phys. Chem. Solids **35**, 1587 (1974).

[28] *American Institute of Physics Handbook 1972,* 3rd ed., edited by D. E. Gray (AIP, New York, 1972).

[29] J. T. Lewis, A. Lehoczky, and C. V. Briscoe, Phys. Rev. **161**, 877 (1967).

[30] S. G. Louie, S. Froyen, and M. L. Cohen, Phys. Rev. B **26**, 1738 (1982).